

# A novel method for simultaneous measurement of internal and external hydrodynamic force of self-propelled robotic fish

Li Wen<sup>1</sup>, Tianmiao Wang<sup>1</sup>, Jianhong Liang<sup>1</sup>, Guan hao Wu<sup>2</sup>

**Abstract**—Hydrodynamic investigation of carangiform robotic fish has been carried out by using a novel experimental method. The laboratory robotic fish model which follows an exact replica of Saithe, is self-propelled on a servo towing system. The forward towing speed is determined by the fluid force acting upon the robotic fish, as the fish undulate its body in the water. The importance of the self-propelled method which allows for simultaneous measurement of internal and external force and flow analysis of robotic fish has been demonstrated in the hydrodynamic experiment.

## I. INTRODUCTION

The comparative biomechanics and physiology of moving through water has long attracted the attention of both biologists and engineers. Until recently, experiments with the state-of-the-art particle image velocimetry (PIV) techniques[1] have provided insights into mechanisms of live fish hydrodynamic force generation, kinematics. Researchers also use electromyography experiments on swimming fish to obtain internal muscle activation (electromyogram (EMG) activity) along the body[2]. However, governing kinematics parameters cannot be systematically varied with live fish[3]. Robotic model experiments can not only help engineers creating high thrust performance biomimetic fish-like vehicle[4][5], but also providing assistance to reveal the inherent mechanism of biological hydrodynamic performance[6][7].

Although a variety of different free swimming autonomous robotic fish designs and devices that exploit fish-like swimming techniques have been introduced [8]~[11], hydrodynamic experiments for testing swimming performance can only be taken by the use of laboratory model that allows specific movement patterns as well as force measurement. Fig.1 summarizes two main conventional approaches for robotic platforms which are useful for the researches of hydrodynamics force measurement. As can be seen in Fig.1A, robotic fish model is attached to a strut which holds the robotic model vertically from the towing carriage above[12][13], or alternatively fixed to a place in the water tunnel[14]. Thus, forces can be

measured by the transducers while the robotic fish model was active towed at a preset speed, or given an oncoming flow velocity in the water tunnel. However, the robotic fish is not self-propelled, but moves at constraint imposed flow, in most cases, there is no equality between the thrust and drag .

In Fig.1B robotic fish swims at a passively speed on a low-friction bearing guide rail while taking a certain movement, the thrust force equals the model drag force coupled with the strut drag (denoted by  $D_s$  in fig.1B)[5][15]. However, such kind of passive towing system has two defects indicated as follows: 1. Affiliated mechanical parts under the force transducer, as shown in Fig.1 (e.g. slide block, strut, et al.), would result in an increase to inertia mass of robotic fish model, consequently the acceleration of robotic fish will be much smaller than that of real self-propelled situation[16]; 2. It no longer has the capacity of setting a given speed for the robotic model, this results in difficulties to measure the robotic fish's drag force.

It is indicates that the hydrodynamic thrust performance test should be conducted under condition of self-propelled[17]. Take both active towing system and passive towing system (as described in fig.1) into consideration, in this paper, we will propose a novel experimental method based on force-feedback control technique, which combines the advantages of two methods proposed in fig.1.

As the majority of fishes use body/caudal fin (BCF) undulations for propulsion, only about 12% of 450 extant fish families use other types of kinematics[18], carangiform swimmers typically achieve a relatively high Reynolds number ( $10^5 \sim 10^6$ ) which is well within the inertial regime where viscous forces are negligible and inertial forces dominate the hydrodynamics. In this paper, we will focus on hydrodynamic test of carangiform robotic fish, and propose a novel method for simultaneous measurement of power consumption, external force, as well as flow visualization of a self-propelled robotic fish .

The remainder of this paper is organized as follows, in section II. A brief description of the carangiform robotic fish design and self-propelled experimental system is firstly introduced. Calibration and relative result of the experimental apparatus is presented in section III. Hydrodynamic result of self-propelled robotic fish is given in section IV, finally we summarized our research and findings, present the discussions of our work, and online for future studies.

Manuscript received March 10, 2010. This work was supported in part by National Outstanding Youth Science Foundation support projects, China, under contracts 60525314.

Li wen, Tianmiao Wang are with the robotic institute in school of Mechanical Engineering and Automation, Beihang University, Beijing 100083, P.R.China, author for correspondence: phone:86-010-82338033; fax:86-010-82338271.

Guanhao Wu is with the State Key Laboratory of Precision Measurement Technology and Instruments, Department of Precision Instruments, Tsinghua University Beijing, China.

Author for correspondence: [alex.wenli@gmail.com](mailto:alex.wenli@gmail.com)

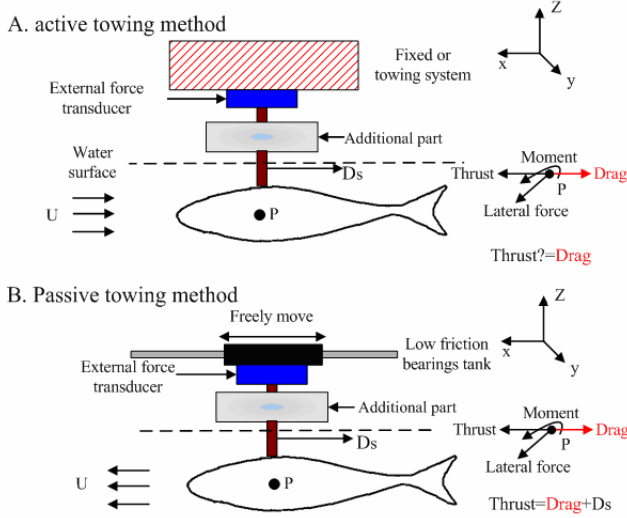


Fig.1 Schematic view to illustrate two main conventional categories of flexible fish hydrodynamic test method

## II. MATERIALS AND METHODS

### A. Experimental apparatus

#### 1) Robotic fish design

The robotic mechanism has total length of 0.59m and consists of a streamlined main body capable of flexing and a rigid propulsive tail fin (See Fig.2a). The outer shape of the robotic fish is an exact replica with the shape of a typical carangiform swimmer: Saithe (*Pilachius Virens*) whose body shape parameters have been provided [19]. In addition, great effort was made to imitate the internal mass distribution of robotic fish body following the real Saithe.

The mechanism is a high-precision assembly of 4 links made anodized aluminum and covered with foams, and is covered by silica so as to reduce friction drag while swimming. Fig. 2a provide details of the robotic fish implementation, which is consist of mechanical links and artificial “muscle”, each capable of relative rotation with respect to its neighboring links [20]. All the links are independently controlled by a motion coordinator TRIO MC206, belts transmits the motion to individual links with minimal frictional forces owing to bearings which are assemble on the shafts as shown in Fig.2b. As shown in Fig.2(above left) relative link lengths were computed to approximate a given smooth, time varying body-wave curve using geometric optimization [21]. Optimized results shows that the best optimized link-length ratio is  $l_1:l_2:l_3:l_4=0.36:0.24:0.22:0.18$ ,  $l_j$  ( $j=1,2,..4$ ) which represents the length of  $j$ th link of the robotic fish. It should be noted that  $l_4$  represents the chord length of robotic fish.

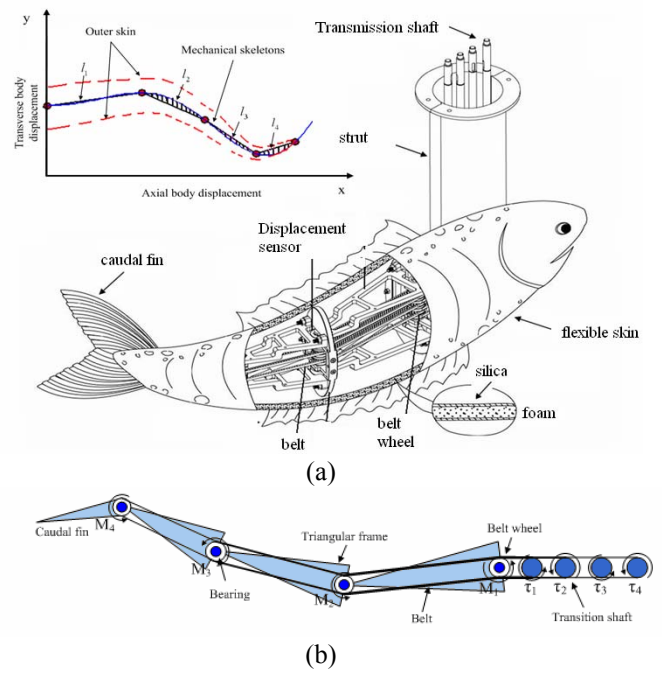


Fig.2. (a) Schematic view of robotic Saithe and actual fitting curve versus reference body wave in the robotic fish (b) Actuation mechanisms of relative rotations of the robotic links

#### 2) Power consumption measurement

As shown in Fig.3, a pair of activating belt per motor which can drive the mechanical links to move separately. Belt force and torque will be transmitted by 4 shafts as can be seen in Fig.3, which run through the vertical strut and finally get into the fish body and drive the individual link. Belts are connected to each motor wheel which is connected with motor output axis. For the  $i$ th motor corresponding to  $i$ th mechanic link, the upside belt is pulled in while registering force  $N_{i1}$ , and the downside is paid out while registering force  $N_{i2}$  (see fig.3). While the idler presses the outside of the synchronous belt firmly. By mounting load cell on the idler,  $N_{i1}$  and  $N_{i2}$  can be measured. The relations of  $N_{i1}$ ,  $N_{i2}$  and the bending moment  $M_i$  is:

$$M_i = \left( \frac{N_{i1}}{(1 + e^{2r\theta}) \cdot \sin \theta} - \frac{N_{i2}}{(1 + e^{-2r\theta}) \cdot \sin \theta} \right) \frac{d}{2} \quad (1)$$

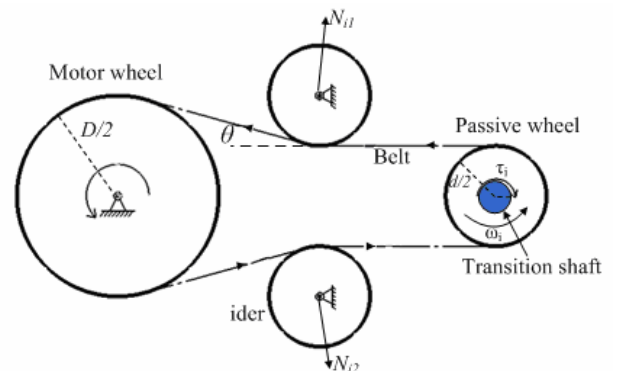


Fig.3 Internal force measurement apparatus, where belts and force transducers are clearly shown.

Where  $r$  denotes the friction coefficient between belt and idler ( $r=0.29166$ );  $\theta$  represents the wrap angle of the transmission belt on the idler;  $d$  denotes the diameter of passive wheel. The instantaneous power is found as  $P_j=M_j\omega_j$ , where the  $\omega_j$  denotes the angular speed of each motor. Angular velocity is obtained through the differential value of potentiometer, where  $\omega_j=d(\theta_j)/dt$ . The overall instantaneous power is calculated as the sum of the input power in all four joints and integrated to find the average power which is represented by  $P$  as shown in equation 11 over a undulatory cycle under condition of self-propelled swimming. The total average power consumption of fish body within a period can be expressed as:

$$P = \frac{\int_0^T \sum_{i=1}^{i=4} M_i(t)\omega_i(t)dt}{T} \quad (2)$$

### 3) Self-propelled method and external force measurement

Fig.4 shows the mechanical components of the self-propelled robotic fish experimental apparatus, while the robotic fish model, multi-component force measurement sensor become an integrate part which is fixed on the towing system as shown in Fig.4, the force about the center of the multi-component force sensor will satisfy the following:

$$F_x + F_{sx} + D_s = (m_f + m_a) \frac{dU'}{dt} \quad (3)$$

Where  $F_x$  denotes axial net force of robotic fish,  $F_x, F_y, M_x$  denotes instantaneous force measured by multi-component force sensor in the direction of x (forward direction), y (lateral direction) and torque at the center of force sensor  $P'$ , respectively.  $m_f$  denotes the mass of the robotic fish,  $m_a$  denotes the mass of the additional parts under the force sensor apart from the robotic fish. The mass of additional parts includes: the inherent mass of the force sensor, the mass of motor as well as the mechanical transmission system and mass of strut.  $U'$  represents the forward speed at point  $P'$ . As the force sensor is fixed on the towing system, therefore  $U'$  also denotes the forward speed of towing system.

$$F_x = m_f \frac{dU(t)}{dt} \quad (4)$$

As equation 4 represents the free swimming condition of the robotic fish in forward direction, and if the speed of towing system  $U'$  equals the right-hand sides, the above equation can be replaced by equation 5, then equation 6 derived.

$$\frac{dU'}{dt} = \left( \frac{F_{sx} + D_s}{m_a} \right) \quad (5)$$

$$F_x + F_{sx} + D_s = (m_f + m_a) \left( \frac{F_{sx} + D_s}{m_a} \right) \quad (6)$$

$$F_x = m_f \left( \frac{F_{sx} + D_s}{m_a} \right) = m_f \frac{dU'}{dt} \quad (7)$$

For  $F_x$  denotes the same as that in equation 4, thus  $U=U'$ , the robotic fish fixed in a towing system will satisfy the free swimming (e.g. self-propelled) in the forward direction, To relate the force to towing speed, we represent equation 5 by the time-discrete form as shown in equation 8.

$$[U(t) - U(t - \Delta t)] / \Delta t = \frac{F_{sx} + D_s}{m_a} \quad (8)$$

Above equation is now to govern the forward speed  $U$  with the force feedback by the over sensor. Even a small change in  $F_{sx}$  will be fed back, corresponding change in forward speed  $U$  by servo towing system. The lateral force  $F_{sy}$  and the moment  $M_{sxy}$  can also be measured while at the quasi-steady state.

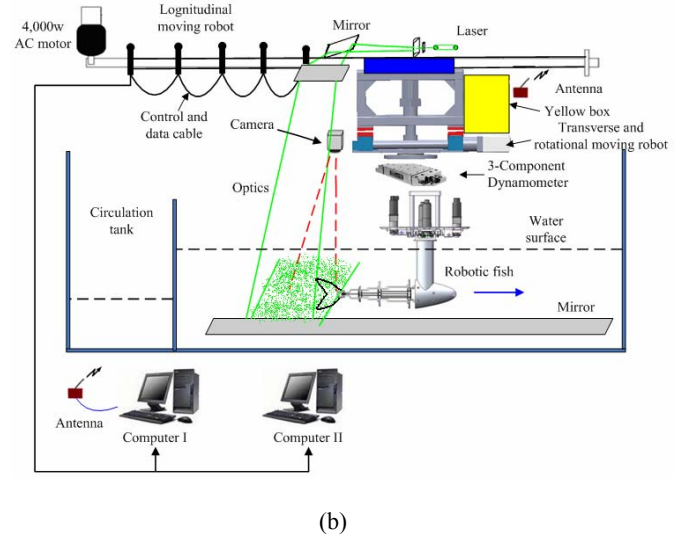


Fig.4 Schematic view of whole system for self-propelled robotic fish model, where the yellow box represent shelf for robotic fish power supply, motion control, amplifier and data acquisition system.

The experimental apparatus which consist of robotic fish and its internal force measurement load cells, 3-component piezoelectric force sensor, servo towing system, laser system and camera used for flow visualization, is built above a water tank which has the following dimensions: 7.8m×1.2m×1.1m. To implement such a complicated instrument, as shown in Fig4, the robotic fish is mounted vertically under the Kistler quartz crystal 3-component sensors 9254C which has got a natural frequency of 3 kHz, high rigidity of 500N/um, and sensitivity of 0.005N in the forward direction. Fish's center of mass is vertically below the center of the Kister, the robotic fish model together with Kislter and accurately fixed on the servo towing system. Forward force acting on the center of mass at time t will be  $F_{sx}(t)$ , this force can now be used to

update the forward velocity, rather than using the newly computed force directly in equation 8, a weighted average force is used instead by the following:

$$\bar{F}_{sx}(t) = \sigma F_{sx}(t) + (1 - \sigma) F_{sx}(t - \Delta t) \quad (9)$$

Where  $\sigma$  is the weighting factor commonly chosen to be between 0.5 and 1.0, the actual experiment result has shown that the optimal choice for  $\sigma$  is 0.85, while below this value, the whole towing system becomes unstable and waking, whereas increasing  $\sigma$  from 0.85 to 1 reduce the accuracy of force feedback velocity. Using the weighted force as given above, equation 9 can be rearranged to give as in the following equation:

$$U(t) = \left( \frac{\bar{F}_{sx} + D_s}{m_a} \right) \Delta t + U(t - \Delta t) \quad (10)$$

The output of robotic fish internal force as well as external force measured by Kistler are recorded in computer I (see Fig.4) through a connecting cable using CAN bus, simultaneously, the forward force  $F_{sx}$  will be transmitted to the motion coordinator Trio MC206 for speed control via equation 10. The particle image will be transferred through another cable to computer II for flow visualization analysis, while the laser sheet will pass through the middle of the robotic fish caudal fin, a high speed CCD camera covered by an optical band pass filter was used to capture the particle image. As described above, the internal and external force measurement as well as PIV visualization can be implemented simultaneously under condition of self-propelled.

### C. Force calibration

As all the measurement system including the internal and external force sensor was set above the water, the apparatus was calibrated and evaluated by add known external static load and dynamic load in the form of weight lifted through pulleys, as shown in Fig.5a.

The performance of the belt force sensors were checked by applying a known load to the cable attached to the robotic fish's tail (with the servo motors of robotic fish active to prevent body motion), while the force increase by each pair of belt force sensors was fully recorded. This test allows direct comparison of the actual measured force with the predicted force calculated, result of linearity is better than 2.2%. The dynamic power calibration was conducted as following: the line passes through a low-friction idler pulley located at a distance of 0.3m to one side of the tail and connects a hanging known weight. Subsequently, each link of the robotic fish was commanded to make undulate movement at certain amplitude and frequency, the displacement data was measured and recorded through the potentiometer built-in the fish model. Each calibration process take a accurate time of 19 seconds, and after the initial transients (4 seconds) had died down and steady state

was obtained. Entire calibration process was performed for over 2 months in order to test its repeatability and the result is considered to be accepted.

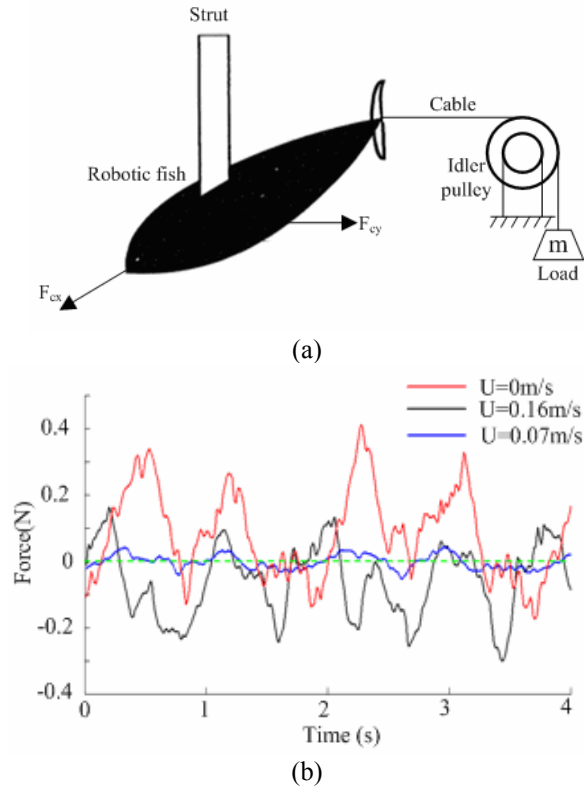


Fig.5 schematic view of force calibration setup, (b) External force dynamic calibration result for 3 distinct runs, run parameters:  $h=0.1, f=0.6\text{Hz}, \lambda=1.04$  at  $U=0\text{m/s}, 0.07\text{m/s}, 0.16\text{m/s}$ , separately.

Fig.5b shows the time history of the instantaneous net forward force at varied known towing speed, where dashed green line indicate that thrust equals drag force, the positive and negative values indicate that the net forward force is of thrust- and drag-type, respectively, for all towing speed, the net force in each cycle shows two peaks, this result is in agreement with experimental observations[22]. As active towing speed  $U$  is set as  $0\text{m/s}$ , the average net force is  $0.0899\text{N}$ , i.e. thrust force exceeds the drag force and net force on the fish body is in the direction of forward (thrust-type), as towing speed increase up to a threshold  $U(U=0.07\text{m/s})$  at which drag-type is observed, where the average net force is  $-0.005\text{N}$ . Further increase of  $U(U=0.16\text{m/s})$  leads a negative mean force up to  $-0.0688\text{N}$ .

## III. RESULT

### A. Kinematics and force result of self-propelled

We present one typical case of robotic fish's self-propelled experiment, where the fish swimming from rest cruise mode, as approximately fitted from observed results in live swimmer[2], kinematics for robotic fish is given as follows:

$$h_{acc}(x, t) = H_{\max} a(x) a(t) \sin(kx - \omega t) \quad (11)$$

Where:

$$a(x) = \begin{cases} 0 & x \leq 0.33L \\ c_1 \left( \frac{x/L - 0.33}{1 - 0.33L} \right) + c_2 \left( \frac{x/L - 0.33}{1 - 0.33L} \right)^2 & x > 0.33L \end{cases}$$

$$a(t) = \begin{cases} \frac{t}{t_0} - \frac{1}{2\pi} \sin\left(\frac{2\pi t}{t_0}\right) & 0 \leq t \leq t_0 \\ 1 & t > t_0 \end{cases}; \quad (12)$$

Where  $L$  represents the fish body length. As equation 21 presents, the robotic fish undulates its posterior part (i.e.  $x > 0.33L$ ) of the body from rest ( $t=0$ ) to steady periodic undulation ( $t > t_0 = 1.0T$ ) after a gently transition process ( $0 < t < t_0$ ). Robotic fish is set to conduct several cycles of undulation under condition of self-propelled, for the following kinematics parametric value: the dimensionless tail end amplitude  $h=0.1$ , and flapping frequency of  $f=0.6\text{Hz}$ , and the body wavelength  $\lambda$  is 1.04.

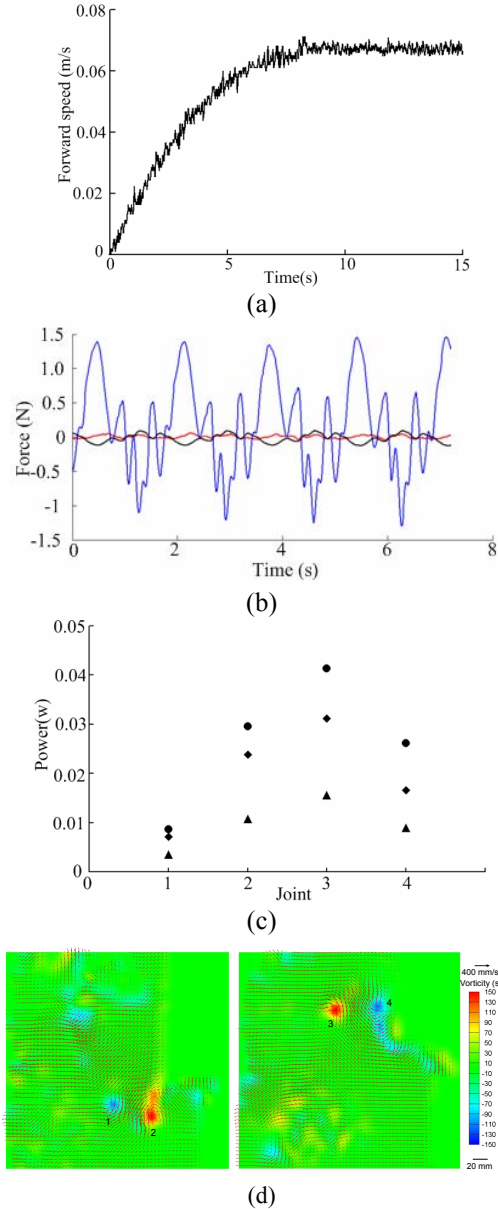


Fig.6 (a) Forward speed of robotic fish under condition of self-propelled. (b) The external lateral force (blue), forward force (red) and moment (black) when steady swimming mode is achieved. (c) Internal mean power to each segment under conditions of self-propelled for 3 runs separately:  $f=0.6\text{Hz}$ ▲,  $f=1.0\text{Hz}$ ◆,  $f=1.4\text{Hz}$ ● at fixed  $h=0.1$  and  $\lambda=1.04$ . (d) Flow patterns generated by the robotic fish.

Fig.6a shows the forward velocity of robotic fish over 15s under condition of self-propelled, during 4~5 cycles of body movement which takes about 8s, the robotic fish reached the steady swimming mode, with a asymptotic mean velocity of 0.072m/s. We can pose the question whether asymptotic mean velocity from self-propelled method is comparable with previous result obtained from active towing method. Consequently, the self-propelled speed is in good agreement with the threshold value ( $U=0.07\text{m/s}$ ) which indicated the thrust balance the drag. Fig.6b shows that after robotic fish has settled into its steady swimming state the lateral force is much bigger than the net forward force, dashed green line indicate the zero force. Moment about center of mass is also shown in Fig.8b. The present power consumption measurements for joint segments are in agreement with conclusions of Rome[23] who measured directly the power consumed by the muscle of live fish along its length. The four link structure of current robotic swimmer replicate to a certain extent the body of live fish, from Fig.6c, under condition of self-propelled, the front part(the first joint) takes about 12%, the middle part(the second joint) takes about 30%, the rear part 58% of the average total hydrodynamic power from 3 distinct runs. The power distribution result can play a guiding role in future robotic fish design, different actuator can provide power for corresponding location along the robotic fish length. Fig.6d shows the flow patterns generated by the robotic fish for above kinematics parametric value. In each flapping cycle, the tail performed two flicks, a flick to its right side and then a flick to its left side. Each flick of the tail generated a pair of vortices. After shedding, the two vortices that formed a pair were located at the same side of the body axis and moved sideways away from the body axis. According to the previous results of carangiform fish swimming, each vortex pair reflected the cross section of a three-dimensional vortex ring. So two vortex rings were generated in each flapping cycle (one ring by right flick and another by left flick). However, the two vortex rings were not linked. It is different from the results reported for the carangiform fish during steady swimming.

## IV DISCUSSION

### A. Methods

The generality of the experimental method discussed here indicates that many broader issues relating to the design and control of biologically inspired underwater robot can be examined using this test method, as means of understanding how external hydrodynamic force is generated, internal power is consumed, and wake structure is formed simultaneously. One the most significant difference between current self-propelled method and that of traditional active towing method is the total number of experimental runs

decreased a lot. Over 600 experiments were conducted on robotic tuna at fixed towing speed[7], however, most experimental runs were abandoned for net forward force is not zero, while current experiment provide every single run self-propelled.

### B. Swimming performance and thrust efficiency of robotic fish

The definition of thrust efficiency of fish-like swimming is controversial and ambiguous[3], and there is previous report on efficiency test for robotic fish for the thrust force can not be measured directly in experiments, because it is impossible to distinguish the fish's body and tail, as both of them provide thrust and drag at the same time. The Froude efficiency  $\eta$  based on Lighthill's elongate body theory[19] (EBT) for steady swimming is given as:

$$\eta = \frac{1}{2}(1 + \beta) \quad (22)$$

And its improved form(EBT-2) which takes into account the slope of fish tail:

$$\eta = \frac{1}{2}(1 + \beta) - \frac{1}{2}\alpha^2(\beta^2 / 1 + \beta) \quad (23)$$

Where  $\beta$  denotes the slip velocity defined as ratio of the steady swimming speed to the body wave speed,  $\alpha$  represents the slope angle of tail. The Froude efficiency of current robotic fish under condition of self-propelled is 59.7% and 57% for the kinematics parameters:  $h=0.1$ ,  $f=0.6\text{Hz}$ , and  $\lambda=1.04$  using EBT and EBT-2, separately, although it is known that both of these two methods overestimate the efficiency. Also currently, the body and tail of robotic fish are treated together as a single undulatory wave for simplified, however, recent findings shown that the caudal fin undergo complex kinematics independent of body in some scombrid fishes (e.g., mackerel, Tuna)[24][25], thus shedding vorticity in different way, and the wake structure has close relationship with thrust performance of live fish. Considering this, more principal parameters besides current kinetic parameters will be taken into consideration to explore optimal swimming performance for a given robotic fish.

### ACKNOWLEDGMENT

This work was supported in part by National Outstanding Youth Science Foundation support projects, China, under contracts 60525314.

### REFERENCE

- [1] Lauder, G. V. and Drucker, E. G., " Forces, fishes, and fluids: hydrodynamic mechanisms of aquatic locomotion," *News Physiol. Sci.*, vol.17, pp.235-240, 2002.
- [2] Videler J J. 1993. *Fish Swimming*[M]. London: Chapman & Hall.
- [3] Iman Borazjani. Numerical investigation of the hydrodynamics of carangiform swimming in the transitional and inertial flow regimes. *J. Exp. Biol.* 2008, 211: 1541-1558.
- [4] Anderson, J. M. and Chhabra, N. Maneuvering and stability performance of a robotic tuna. *Integr. Comp. Biol.* 2002, 42:118-126.
- [5] N. Kato. Control performance in the horizontal plane of a fish robot with mechanical pectoral fins. *IEEE J. Oceanic Eng.* 2000, 25:121-129.
- [6] Bandyopadhyay P R, Beal D N, Menozzi A. Biorobotic insights into how animals swim. *J Exp Biol*, 2008, 211(2):206-214.
- [7] Barrett, D., Triantafyllou, M., Yue, et al. Drag reduction in fish-like locomotion. *J.Fluid Mech.* 1999, 392:183-212.
- [8] Huosheng Hu et al. Design of 3D Swim Patterns for Autonomous Robotic Fish. *In Proc. IEEE/RSJ Int. Conf. Intelligent Rob. and Sys.*, 2006: 2406-2411.
- [9] Li Wen, Tianmiao Wang et al. Fuzzy logic vorticity control of oscillating foil UUV. *In Proc. IEEE/RSJ Int. Conf. Intelligent Rob. and Sys.* 2009:1019-1024.
- [10] Long, J. H., et al. Biomimetic evolutionary analysis: testing the adaptive value of vertebrate tail stiffness in autonomous swimming robots. *J. Exp. Biol.*, 2006, 209:4732-4746.
- [11] G. V. Lauder, E. J. Anderson, J. Tangorra, et al. Fish biorobotics: Kinematics and hydrodynamics of self propulsion. *J. Exp. Biol.*, 2007, 210:2767-2780.
- [12] Bandyopadhyay, P. R., Trends in biorobotic autonomous undersea vehicles, *IEEE J. Oceanic Eng.*, vol.30, pp.109-139, 2005.
- [13] Beal, D. N., Hover, F. S., Triantafyllou, M. S., Liao, J. and Lauder, G. V., "Passive propulsion in vortex wakes," *J. Fluid Mech.*, pp.385-402, 2006.
- [14] Guang-Kun Tan, Gong-Xin Shen, Shuo-Qiao Huang, "Investigation of flow mechanism of a robot fish swimming by utilizing flow visualization synchronized with hydrodynamic force measurement," *Experiments in Fluids*, vol.43, pp.811-821, 2007.
- [15] K. Morgansen, V. Duindam, R. Mason, J. Burdick, and R. Murray, "Nonlinear control methods for planar carangiform robot fish locomotion," *in Proc. IEEE Int. Conf. Robot. Autom.*, 2001, pp. 427-434.
- [16] Carling J, Williams T L, Bowtell G, "Self-propelled anguilliform swimming: simultaneous solution of the two-dimensional Navier-Stokes equations and Newton's laws of motion," *J Exp Biol*, vol. 201, no.23, pp.3143-3166, 1998.
- [17] Sfakiotakis M, Lane D M, Davies J B C, "Review of fish swimming modes for aquatic Locomotion," *IEEE J Oceanic Eng.*, vol.24, no.2, pp.237-252, 1999.
- [18] Iman Borazjani. Numerical investigation of the hydrodynamics of anguilliform swimming in the transitional and inertial flow regimes. *J. Exp. Biol.* 2009, 212: 576-592.
- [19] Lighthill M J, "Note on the swimming of slender fish," *J Fluid Mech*, vol.9, no.2, pp.305-317, 1960.
- [20] Yu J, Tan M, Wang S, Chen E, "Development of a biomimetics robotic fish and its control algorithm," *IEEE Trans Syst Man Cybern Part B: Cybern* vol.34, no.4, pp.1798-1810, 2004.
- [21] J. Yu, L. Wang, "Parameter optimization of simplified propulsive model for biomimetic robot fish. *In Proc. IEEE Int. Conf. Robotics and Automation*, Barcelona, April 2005, pp. 3317-3322.
- [22] Hess, F. and Videler, J. J., "Fast continuous swimming of saithe (*Pollachius virens*): a dynamic analysis of bending moments and muscle power," *J. Exp. Biol.*, vol.109, pp.229-251, 1984.
- [23] Rome, L. C., Swank, D. & Corda, D. 1993 How fish power swimming. *Science* 261, 340{343.
- [24] Lauder, G. V., Tytell, E. D.. Hydrodynamics of undulatory propulsion. *Fish Physiol*, vol.23, pp.425-468, 2006.
- [25] F.E. Fish, G.V. Lauder, "Passive and Active Flow Control by Swimming Fishes and Mammals", *Annu Rev. Fluid Mech.*, vol.38, pp.193-224, 2006.